# Micro-Resonator Soliton Generated Directly with a Diode Laser

*Nicolas Volet,* Xu Yi, Qi-Fan Yang, Eric J. Stanton, Paul A. Morton, Ki Youl Yang, Kerry J. Vahala, and John E. Bowers*

An external-cavity diode laser for 1550-nm wavelength is reported with ultra-low noise, high power coupled to a fiber, and fast tunability. These characteristics enable the generation of an optical frequency comb in a silica micro-resonator with a single-soliton state. Neither an optical amplifier nor a modulator is used in the experiment. This demonstration greatly simplifies the soliton generation setup and represents a significant step forward to a fully integrated soliton comb system.

## 1. Introduction

Coherent optical frequency combs have revolutionized precision measurement with light.[1–3] However, the complex setups needed to generate and stabilize these systems limit their relevance in field-testing scenarios. Combs generated in a micro-cavity[4–6] ("micro-combs") are evolving rapidly, and provide a pathway to miniaturize frequency comb systems. While early micro-combs were subject to instabilities and lacked the critical ability to form femtosecond pulses, an important advancement has been the realization of temporal soliton in optical micro-cavities.[7] First observed in optical fibers,[8] this form of ultra-short pulse formation has been demonstrated across many micro-cavity platforms. The potential to fully integrate frequency comb systems is driving interest in materials such as silica $(SiO_2)$[9] and silicon nitride $(Si_3N_4)$[10–13] that leverage complementary metal-oxide-semiconductor (CMOS) fabrication infrastructures.[14–16] These are also of interest as soliton stabilization[17–19] necessitates certain electronic components.

Temporal optical solitons[20] were first observed in optical fibers.[21] These nonlinear waves balance the group-velocity

Dr. N. Volet, E. J. Stanton, Prof. J. E. Bowers
Department of Electrical and Computer Engineering
University of California
Santa Barbara (UCSB), CA 93106, USA
E-mail: volet@ece.ucsb.edu

X. Yi, Q.-F. Yang, K. Y. Yang, Prof. K. J. Vahala
T. J. Watson Laboratory of Applied Physics
California Institute of Technology
Pasadena, CA 91125, USA

Dr. P. A. Morton
Morton Photonics
3301 Velvet Valley Drive, West Friendship, MD 21794, USA

The ORCID identification number(s) for the author(s) of this article can be found under https://doi.org/10.1002/lpor.201700307

dispersion (GVD) through the optical Kerr effect. For temporal solitons in micro-cavities, a second balance occurs:[7,22] optical loss is compensated by third-order parametric gain[23] provided by an external pump. Micro-cavity temporal Kerr solitons are accordingly "dissipative".[24–27] This technology has now been applied to demonstrate self-referencing,[28,29] dual-comb spectroscopy,[30–32] optical frequency synthesis,[33] distance ranging,[34,35] and optical communications with tremendous bandwidth.[36]

External-cavity diode lasers (ECDLs) are critical for many applications and are frequently used to optically pump micro-comb systems. They can provide single-mode operation with a narrow linewidth, which is crucial for telecommunications. In addition, their emission frequency can be tuned, which is needed for spectroscopy[37] and frequency synthesis.[33] However, they typically emit modest output power. Consequently, most soliton micro-comb systems to date require non-integrated components to boost the pump laser power. Additionally, other functions to enable rapid control of laser power and frequency (acousto/electro-optic modulators)[17–19] have also been necessary, with the exception of few reports,[38,39] where self-injection locking is leveraged.

In this work, we report an ECDL with extremely narrow linewidth, low relative intensity noise (RIN), high output power, and useful spectral tunability. In particular, it emits 70 mW at 1550-nm wavelength, with a Lorentzian linewidth as low as 63 Hz. This level of spectral purity is orders of magnitude better than the current state-of-the-art ECDLs.[40,41] As a very first application for this prototype, a temporal soliton is directly generated and stabilized in a silica micro-resonator, without using an optical amplifier or an external modulator. This drastically reduces the complexity, size, and cost of the system, and is expected to precede a fully integrated source of solitons.

## 2. Methods

### 2.1. Summary of Temporal Soliton Theory

Optical frequency combs can be generated by pumping a micro-resonator with a single-mode continuous-wave (CW) tunable laser.[4] A non-linear Schrödinger-like equation, in its extended form[25] with driving, damping and detuning terms, has proved remarkably successful in modeling the dynamics of these

combs.[7] Soliton solutions to this differential equation can be characterized by the following temporal width:[7]

$$\Delta\tau = c_1/\sqrt{f_0 - f_p} \tag{1}$$

where the parameter $c_1 \equiv \sqrt{\frac{|\partial_f n_g|}{2 n_g}}/(2\pi)$ depends on the group index $n_g$ of the mode, and its dispersion. The resonator cold mode is centered at $f_0$, and $f_p$ is the laser frequency. When optical power is coupled to the resonator, both the optical Kerr effect and the thermo-optic effect contribute to an increase of the refractive index (at least in silica), causing the mode frequency to red-shift. As a consequence, stable comb generation can be obtained only by approaching the pump frequency from the blue side of the resonance ($f_p > f_0$).[42] However, a necessary condition for the generation of solitons is for the pump to be slightly red-detuned relative to the cold resonance ($f_p < f_0$).[43] Note that, particularly in the presence of a soliton, the intensity is not constant throughout the micro-cavity. The soliton resonance is strongly red-shifted, and the pump frequency remains blue-detuned with respect to it.

The upper envelope of the soliton spectral power density can be approximated by:[44]

$$\Im(f) \propto 1/\cosh^2\left[\pi^2\left(f - f_p + \delta\right)\Delta\tau\right] \tag{2}$$

where $\delta$ is the soliton possible self-frequency shift.[45,46] The maximum of the spectrum occurs at $f = f_p - \delta$. Indeed, it does not necessarily coincide with the pump frequency. Integrating Equation (2) and using Equation (1), the time-averaged soliton power follows:[9]

$$\Im_{sol} \propto \sqrt{f_0 - f_p} \tag{3}$$

This expression suggests that the pump-resonance detuning can be servo locked by fixing the soliton power. From Equation (1), this procedure also sets the pulse temporal width.

## 2.2. Ultra-Low-Noise, High-Power ECDL

A schematic of the prototype ultra-low noise (ULN) ECDL is shown in **Figure 1**a. It combines a high performance semiconductor gain chip (GC) and a polarization-maintaining (PM) optical fiber with an integrated custom designed fiber Bragg grating (FBG),[47] which forms one end of the ECDL. The GC consists of a multi-quantum well (MQW) active region grown on an InP substrate. Dielectric layers are deposited on one facet to form a high-reflectivity (HR) coating, defining the other end of the ECDL.[48,49] The opposite end of the GC has both an angled waveguide and an anti-reflection (AR) coated facet to provide extremely low optical reflectivity, suppressing any parasitic Fabry-Perot reflections and supporting ULN operation. The light emitted from the GC is coupled to the PM fiber via an AR coated lensed fiber.

The ECDL design is optimized to provide ULN performance together with extremely stable single-mode operation.[50] The temperature of the GC and that of the FBG are independently controlled, which allows for coarse frequency tuning. They are packaged in an extended butterfly mount. The present ECDL does not include any moving parts and its footprint is greatly reduced compared to benchtop ECDLs with a piezo-controlled fre-
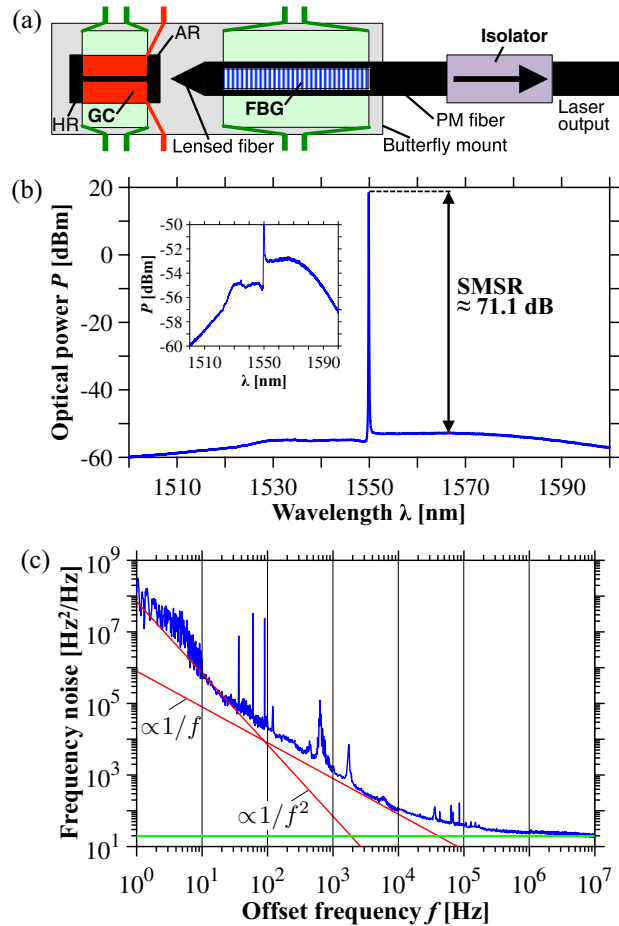


**Figure 1.** a) Top-view schematic of the ECDL used in this work. Pads of the butterfly package drawn in red are for current injection to the GC, and those in green are for temperature control. b) Optical spectrum measured at 525 mA and with $T_{GC} = T_{FBG} = 20\,°C$. The inset is close-up view of the amplified spontaneous emission. c) Corresponding frequency noise. Red lines are proportional to $1/f$ and $1/f^2$, respectively, and the green line indicates the white noise floor.

quency tuning mechanism.[51] These are inherently less robust, as their cavity alignment is very sensitive to temperature fluctuations and vibrations. A PM optical isolator (OZ Optics) with $\approx 60$-dB isolation is spliced to the output fiber to preserve the stability of this device against optical reflections. Note that back reflections from the micro-resonator could be leveraged to further reduce the laser linewidth,[52] so that an isolator may not be necessary for soliton generation. This ECDL has a threshold near 40 mA, and an output power of 70 mW is measured after the isolator with a drive current of 525 mA. At this current level, the side-mode suppression ratio (SMSR) is >70 dB, as seen in Figure 1b. The inset of Figure 1b is a close-up view of the amplified spontaneous emission (ASE). On the red side of the lasing peak, the ASE is $\approx 1.5$ dB higher than on the blue side. This asymmetry can be understood from the non-linear interaction between the optical field and the carrier density in the QWs.[53,54] Specifically, the beating between the intense lasing mode and the ASE modulates the (complex) refractive index, which induces extra gain at longer wavelengths.

ADVANCED
SCIENCE NEWS

www.advancedsciencenews.com

LASER
&PHOTONICS
REVIEWS

www.lpr-journal.org

The frequency noise is measured at 525 mA with an automated system (OEwaves, model OE4000). As seen in Figure 1c, a white noise floor of $\approx 20$ Hz$^2$ Hz$^{-1}$ is obtained for frequencies greater than $\approx 10^6$ Hz. This relates[55] to a Lorentzian 3-dB linewidth of $\approx 63$ Hz. The low linewidth of this laser is due to its long external cavity length, high storage of photons within this cavity,[56] and operation on the long-wavelength side of the FBG reflection.[57,58] In the frequency range 30 Hz–2 kHz, where the $1/f^2$-noise and the $1/f$-noise dominate, several distinct peaks can be seen in Figure 1c. They are inherent to the noise from the electronics of the OEwaves measurement system. On the other hand, contributions in the range 1–10 Hz come from the temperature controllers.

RIN measurements were also performed using the OEwaves system. Over the entire offset frequency range from 10 Hz to 100 MHz, the measured RIN is equal to the noise floor of the equipment, thus only providing an upper limit to the RIN of the ECDL. The noise floor of the OE4000 unit varies from −130 dBc Hz$^{-1}$ at 10 Hz, down to almost −160 dBc Hz$^{-1}$ at 100 kHz, and is then flat out to 100 MHz. This RIN performance is comparable to state-of-the-art low-noise ECDLs in the C band,[40,41] while the linewidth demonstrated by the device in the present experiments is $\approx 15$ times narrower.

To characterize the tuning range, the ECDL output is sent through a fiber-based unbalanced Mach–Zehnder interferometer (MZI) with a free spectral range (FSR) of $\approx 40$ MHz. By slowly ramping the current in the ECDL, a normalized frequency change of $\approx 20$ MHz mA$^{-1}$ is measured, and the widest mode-hop-free tuning range is 2.28 GHz (or 18.3 pm). This is much narrower than specified for commercial benchtop ECDLs, but as will now be shown, the tuning speed is at least 2 orders higher. A time-harmonic voltage is applied across the ECDL, with a modulation frequency $f_m = \omega_m/(2\pi)$, and the MZI output is connected to a high-speed photo-detector and recorded with an oscilloscope. The current through the ECDL can be expressed as $I(t) = I_0 + \Delta I(t)$, with a mean value $I_0$, a modulation $\Delta I(t) = I_{0p} \cos(\omega_m t)$, and a current peak amplitude $I_{0p}$. This causes the laser frequency to vary harmonically, with a peak deviation $\Delta f_{max}$. For $f_m \ll \Delta f_{max}$ and small-signal modulation ($I_{0p} \ll I_0$), the intensity out of the MZI can be written as:[37]

$$\mathfrak{I}_{MZI} = \mathfrak{I}_0 + \Delta\mathfrak{I}_{MZI} = (\mathfrak{I}_0 + \Delta\mathfrak{I}_{IM})(1 + \Delta\mathfrak{I}_{FM}/\mathfrak{I}_0) \quad (4a)$$

where $\mathfrak{I}_0$ is the unmodulated intensity, and:

$$\Delta\mathfrak{I}_{IM} = m\mathfrak{I}_0 \cos(\omega_m t + \varphi_{IM}) \quad (4b)$$

$$\Delta\mathfrak{I}_{FM} = R\mathfrak{I}_0 \cos\left[2\pi \frac{\Delta f_{max}}{FSR} \cos(\omega_m t + \varphi_f) + \varphi_{FM}\right] \quad (4c)$$

Equation (4b) represents the spurious intensity modulation (IM) as the laser frequency is chirped, and $m$ is the IM index. In contrast, Equation (4c) arises from frequency modulation (FM). The parameter $R$ is related to the MZI couplers, and the $\varphi$'s are phase constants. In the present measurements, the modulation frequency is set to $f_m = 1$ MHz and the amplitude $I_{0p}$ is varied up to 61 mA. An example is shown in **Figure 2a** for $I_{0p} = 42.7$ mA. The intensity out of the MZI is fitted with Equation (4a) to extract $\Delta f_{max}$. The FM efficiency is then found from $\eta_{FM} \equiv \Delta f_{max}/I_{0p}$.
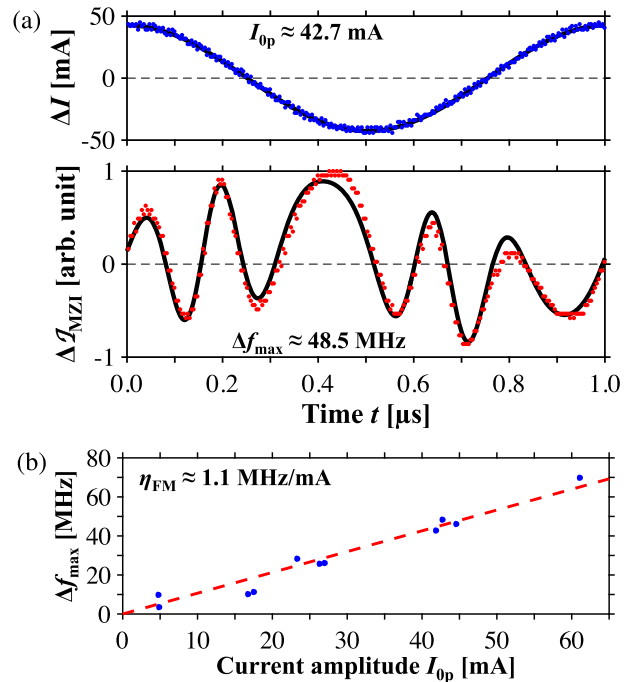


**Figure 2.** a) Upper, small-signal current modulation of the ECDL for a certain value of $I_{0p}$, and lower, corresponding intensity variation out of the MZI fitted (in black) with Equation (4a). b) Peak frequency deviation $\Delta f_{max}$ obtained for different current amplitudes $I_{0p}$. The FM efficiency is extracted from the slope of the linear fit (in red).

Note that for $f_m$ below 50 MHz, temperature-induced FM effects are expected to be significant.[59,60] Specifically, $\eta_{FM}$ is expected to decrease as $f_m$ increases from DC to 50 MHz. It is then usually relatively constant up to the relaxation resonance. Figure 2b demonstrates frequency tuning speed above 280 MHz µs$^{-1}$. Significantly, a frequency deviation of 40 MHz (required for soliton generation in a silica micro-disk), can be generated with a current amplitude of 40 mA. Data in Figure 2b are well fitted with a straight line, and the slope is $\eta_{FM} \approx 1.1$ MHz mA$^{-1}$.

## 2.3. Silica Micro-Resonator

The thermally-grown silica micro-disk resonator is fabricated on a Si substrate with a technique reported elsewhere.[61] Its diameter is 3 mm, which corresponds to an FSR of 22 GHz. The resonator profile is a wedge with an angle near 30° and a thickness of 8 µm. This geometry can simultaneously provide anomalous GVD,[9,62] high quality factor and minimal mode crossing. The latter effect is known to hinder soliton formation.[63] Light is evanescently coupled to the micro-resonator via a tapered fiber.[64–66] From transmission measurements, the resonance used in this work for soliton generation has a loaded, full-width-at-half-depth (FWHD) linewidth of 1.2 MHz, and therefore a total quality factor $Q_{tot} \approx 160$ M. The micro-resonator is under-coupled[67] in the measurement and has an intrinsic value $Q_i \approx 260$ M.

**ADVANCED
SCIENCE NEWS**

www.advancedsciencenews.com

LASER
& PHOTONICS
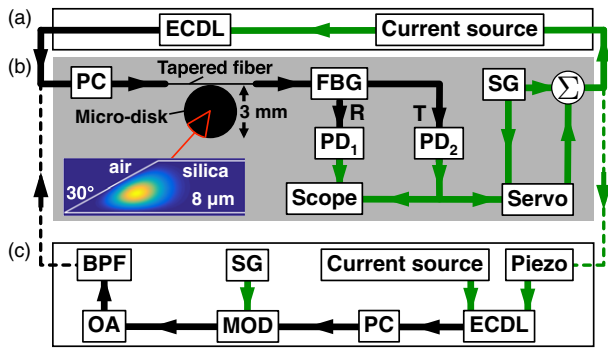REVIEWS

www.lpr-journal.org

**Figure 3.** a,b) Schematic of the setup used in this work for soliton generation and locking without an OA. Black and green lines represent optical and electrical paths, respectively. A cross-section schematic of the micro-disk resonator and its wedge profile is shown in (b), with intensity pattern simulated for the fundamental mode. Alternatively, for soliton generation with a piezo-controlled ECDL, part (a) is to be replaced by part (c).

## 2.4. Setup for Soliton Generation

**Figure 3**a–b shows a schematic of the setup used for soliton generation and locking with the ECDL described in Section 2.2. The ECDL is driven by a low-noise current source (Newport LDX-3620B). A signal generator (SG, Keysight 33522B) produces a local oscillation (LO) used to modulate the voltage supplied to the ECDL, and thereby its emission frequency. The output of the ECDL is connected to a polarization controller (PC, Thorlabs FPC560), and the output of the tapered fiber is connected to a FBG. Its reflection port (R), with a 0.1-nm pass-band, transmits the pump laser light which is sent to a photo-detector (New Focus 1811, labeled $PD_1$) and monitored on an oscilloscope. In contrast, the transmission port (T) of the FBG acts as a notch filter and suppresses the pump by 25 dB, so that only the light produced by comb emission and the ASE are detected by $PD_2$. Part of this photo-current is recorded on the oscilloscope, and the remainder is sent to a servo controller (Vescent D2-125) that subtracts a constant offset. The resulting difference serves as the error signal for a feedback-locking loop[9,17] essentially based on Equation (3).

Once the pump frequency reaches the red side of the cold resonance (prerequisite for soliton generation, see Section 2.1), the SG sends a digital signal to the servo to engage the locking loop. The servo controller includes an op-amp integrator. To establish a stable loop, it forces a null at its input by integrating the error signal within a 10-kHz bandwidth. Its output is a correction voltage signal that is fed back to the ECDL current source, combined with the LO. By adjusting the offset value, states with different soliton numbers can be generated.[17] As shown in the next Section, the

tuning and locking parameters were optimized to guarantee the generation and stabilization of a *single*-soliton state.

The conventional methods for generation of solitons using piezo-controlled ECDLs can be understood by replacing part (a) with part (c) in Figure 3. Specifically, two common methods have been developed to overcome the thermal instability and generate solitons. They are based on abrupt changes of either the pump power[9,10,17,18] or the pump frequency,[19] and referred to as "power kicking" or "frequency kicking", respectively. These changes occur over timescales that are faster than the thermal time constant of the micro-resonator. Referring to Figure 3c, the pump is typically provided by a benchtop ECDL with a piezo-controlled frequency. The servo feedback is applied to the piezo-controller, and not to the current source like in the procedure described above. For power kicking, the modulator in Figure 3c consists of a combination of acousto-optic and electro-optic modulators (with modulation frequencies up to $\approx$100 MHz). In contrast, the frequency kicking protocol is achieved by manipulating the single sideband from a quadrature phase shift keying (QPSK) modulator driven by a fast-tuning voltage-controlled oscillator (VCO). In both protocols, the modulators are controlled by an extra SG and have optical insertion loss of a few dB. An optical amplifier (OA) is thus inevitably required to boost the pump power. A band-pass filter (BPF) is also preferred to suppress the undesired ASE from the OA. Note that AOMs and QPSKs require a specific polarization for optimal operation, so that an extra PC is also needed. These instruments dramatically increase the footprint, power consumption, and cost of the micro-comb system. In this work, we are able to eliminate these bulky components by implementing a frequency-kicking protocol directly with an ECDL.

## 3. Results and Discussion

The ECDL is driven at 350 mA where its output power is 42 mW, and the power coupled into the tapered fiber is 34 mW. **Figure 4** shows the evolution of the pump power $P_1$ measured after the micro-resonator, as the pump frequency $f_p$ is linearly tuned from the blue to the red side of the resonance. Also shown is the generated comb power $P_2$. Up to $t_1$, $f_p$ is so far from resonance that it does not couple significantly to the micro-disk and $P_1$ is relatively constant. This situation changes near $t_1$ where a reduction of $P_1$ is observed as more light couples to the micro-disk. By $t_{2.1}$, the power coupled to the resonator eventually reaches threshold for parametric oscillation, leading to the onset of a primary comb and a sharp increase of $P_2$. From $t_{2.1}$ to $t_3$, $P_1$ further decreases as more pump power is coupled to the resonator, and between $t_{2.2}$ and $t_3$, $PD_2$ is saturated. Heating of the resonator induces the overall triangular-shaped profile of the pump power transmission.[42] Upon arriving at the edge of the blue-detuned side, the pump frequency is kicked a few MHz to the red-detuned side for a few µs, which induces the soliton state in the resonator. Finally, at $t_4$, *i.e.* a few hundred µs after the scanning, the servo loop is engaged to adjust $f_p$, so as to lock the soliton state indefinitely against thermal drifting. Variations in $P_2$ are further suppressed, suggesting from Equation (3) that the pump-resonance detuning is indeed stabilized.

To confirm soliton generation, the light output from the T-port of the FBG in Figure 3b is sent to an optical spectrum analyser
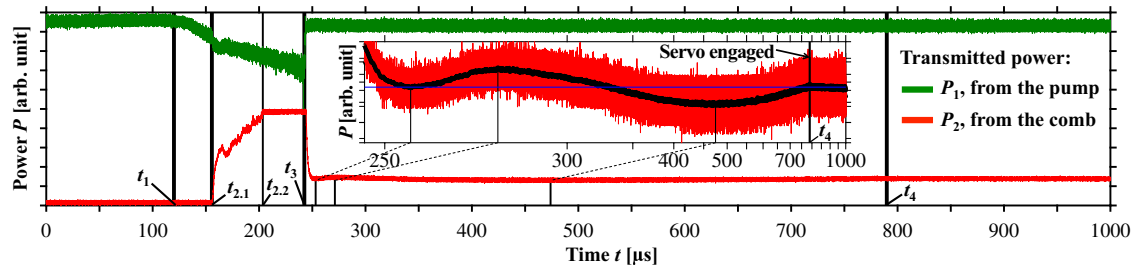
To overcome the thermo-optic effect so that the pump laser frequency is red-detuned relative to the cavity resonance for soliton generation requires rapid tuning over frequency spans as large as 40 MHz at rates in the range of 0.1–2 MHz µs⁻¹.[17] This range and rate are readily achievable with the ECDL. As an aside, rates in the range of 0.3–3 MHz µs⁻¹ are required in SiN combs[18] and also of reach for the ECDL.

**Figure 4.** Frequency tuning leading to the generation of a single soliton, and its subsequent locking. The green and the red curves are the transmitted power from the pump and from the comb, respectively. The inset shows a close-up view of the thermal drift and the soliton locking. The thick black line is a moving average, and the horizontal scale is logarithmic.
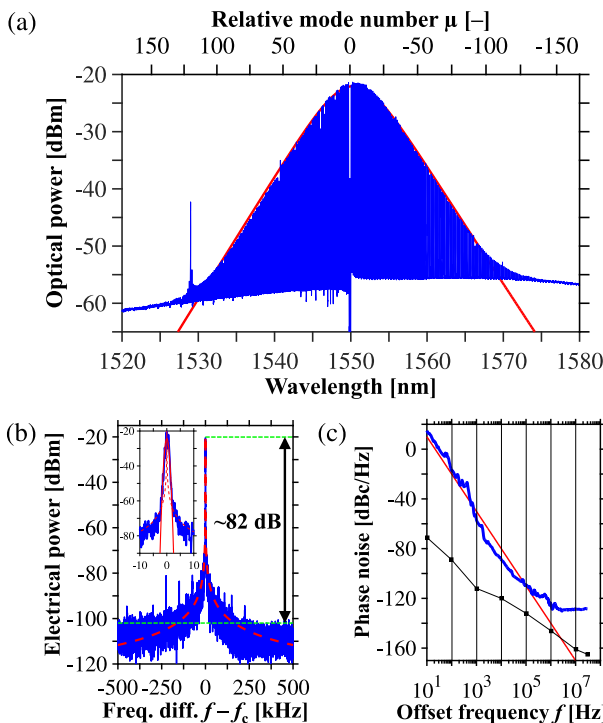


**Figure 5.** a) Optical spectrum measured in the single-soliton regime. The red line is a fit according to Equation (2). b) Corresponding RF electrical spectrum, with $f_c \approx 22.02$ GHz, fitted with a Lorentzian (dashed red). The inset shows the central part, fitted with a Gaussian (solid red). The bottom green line indicates the noise level. c) Phase noise spectral density. The red line is proportional to $1/f^3$ and black squares indicate the instrument sensitivity.

(OSA, Yokogawa AQ6370). It is seen in **Figure 5**a that the spectral envelope is relatively smooth, without significant mode crossings. However, an intensity spike with an amplitude 17 dB above the ASE level is centered near 1529 nm (corresponding to a relative mode number $\mu = 120$). This spectral feature is a signature of a dispersive wave, which in the present case occurs from the interaction of the soliton with different transverse modes in the micro-resonator.[46,68,69] Equation (2) provides an excellent fit for the remainder of this spectrum, and leads $\Delta\tau \approx 196$ fs, and $\delta \approx 60$ GHz. The obtained temporal width is within the range of values (125–215 fs) reported in ref. [44]. The value obtained for $\delta$ indicates a red-shifting of the soliton from the pump by nearly

3 FSRs. This self-frequency shift is usually dominated by stimulated Raman scattering,[44–46] with secondary contributions attributed to the spectral recoil caused by the dispersive wave. Here, a single-soliton state[70,71] is directly generated and stabilized. No step-like features are visible in the oscilloscope traces of Figure 4, as these would occur at the transition between different soliton states.

The soliton is further confirmed by assessing the coherence of the generated comb.[72] Indeed, a low-noise and narrow radio-frequency (RF) signal is known to be a necessary signature of stable soliton formation.[7] In the setup, the OSA is replaced by a PD (Finisar) connected to an electrical spectrum analyser (ESA, Rohde & Schwarz, FSUP26) that also measures phase noise. Figure 5b shows the RF electrical spectrum recorded with a 100-Hz resolution bandwidth. The carrier frequency $f_c \approx 22$ GHz corresponds to the comb repetition frequency, i.e., to the beating between neighboring comb lines. These data have a signal-to-noise ratio >80 dB. They are fitted with a Lorentzian, and the 3-dB linewidth is $\approx 25$ Hz. Note that due to fluctuations (temperature, laser power, etc.), a Voigt profile is observed. As a result, the central part is Gaussian with a 3-dB linewidth of $\approx 1.1$ kHz.

Finally, Figure 5c shows the phase noise spectral density of the repetition beat note plotted versus the offset frequency $f$. Between 10 Hz and 100 kHz, i.e., over 4 decades, the phase noise is approximately proportional to $1/f^3$. This can be attributed to a combination of pump laser RIN and frequency noise.[38,73] The detected phase noise is smaller than $-100$ dBc Hz$^{-1}$ for offset frequencies higher than 28 kHz, which is comparable to the data from a previous report,[46] where the silica micro-resonators were pumped with a commercial benchtop ECDL. Beyond 1 MHz, the detected phase noise reaches its floor value of $-129$ dBc Hz$^{-1}$, attributed to the PD shot noise.[38]

## 4. Conclusion

Soliton generation is demonstrated in a micro-resonator with an ultra-low-noise diode laser. A single-soliton state is successfully stabilized by locking the frequency of the pump laser to the power level of the soliton comb. To our knowledge, it is the first time a temporal soliton is realized in a chip-based micro-resonator without an optical amplifier. This demonstration reduces the complexity and cost of soliton experiments, representing a significant step towards soliton comb systems fully integrated on a single chip.

[1] Th. Udem, J. Reichert, R. Holzwarth, T. W. Hänsch, *Phys. Rev. Lett.* **1999**, *82*, 3568.

[2] S. A. Diddams, D. J. Jones, J. Ye, S. T. Cundiff, J. L. Hall, J. K. Ranka, R. S. Windeler, R. Holzwarth, Th. Udem, T. W. Hänsch, *Phys. Rev. Lett.* **2000**, *84*, 5102.

[3] D. J. Jones, S. A. Diddams, J. K. Ranka, A. Stentz, R. S. Windeler, J. L. Hall, S. T. Cundiff, *Science* **2000**, *288*, 635.

[4] P. Del'Haye, A. Schliesser, O. Arcizet, T. Wilken, R. Holzwarth, T. J. Kippenberg, *Nature* **2007**, *450*, 1214.

[5] T. J. Kippenberg, R. Holzwarth, S. A. Diddams, *Science* **2011**, *332*, 555.

[6] A. Pasquazi, M. Peccianti, L. Razzari, D. J. Moss, S. Coen, M. Erkintalo, Y. K. Chembo, T. Hansson, S. Wabnitz, P. Del'Haye, X. Xue, A. M. Weiner, R. Morandotti, *Phys. Rep.* **2017**, *729*, 1.

[7] T. Herr, V. Brasch, J. D. Jost, C. Y. Wang, N. M. Kondratiev, M. L. Gorodetsky, T. J. Kippenberg, *Nat. Photon.* **2014**, *8*, 145.

[8] F. Leo, S. Coen, P. Kockaert, S. P. Gorza, P. Emplit, M. Haelterman, *Nat. Photon.* **2010**, *4*, 471.

[9] X. Yi, Q. F. Yang, K. Y. Yang, M. G. Suh, K. Vahala, *Optica* **2015**, *2*, 1078.

[10] V. Brasch, M. Geiselmann, T. Herr, G. Lihachev, M. H. P. Pfeiffer, M. L. Gorodetsky, T. J. Kippenberg, *Science* **2016**, *351*, 357.

[11] S. W. Huang, H. Liu, J. Yang, M. Yu, D. L. Kwong, C. W. Wong, *Sci. Rep.* **2016**, *6*, 26255.

[12] P. H. Wang, J. A. Jaramillo-Villegas, Y. Xuan, X. Xue, C. Bao, D. E. Leaird, M. Qi, A. M. Weiner, *Opt. Express* **2016**, *24*, 10890.

[13] C. Joshi, J. K. Jang, K. Luke, X. Ji, S. A. Miller, A. Klenner, Y. Okawachi, M. Lipson, A. L. Gaeta, *Opt. Lett.* **2016**, *41*, 2565.

[14] G. Roelkens, A. Abassi, P. Cardile, U. Dave, A. de Groote, Y. de Koninck, S. Dhoore, X. Fu, A. Gassenq, N. Hattasan, Q. Huang, S. Kumari, S. Keyvaninia, B. Kuyken, L. Li, P. Mechet, M. Muneeb, D. Sanchez, H. Shao, T. Spuesens, A. Z. Subramanian, S. Uvin, M. Tassaert, K. van Gasse, J. Verbist, R. Wang, Z. Wang, J. Zhang, J. van Campenhout, X. Yin, J. Bauwelinck, G. Morthier, R. Baets, D. van Thourhout, *Photonics* **2015**, *3*, 969.

[15] M. L. Davenport, S. Skendžić, N. Volet, J. C. Hulme, M. J. R. Heck, J. E. Bowers, *IEEE J. Sel. Top. Quantum Electron.* **2016**, *22*, 3100111.

[16] A. Spott, E. J. Stanton, N. Volet, J. D. Peters, J. R. Meyer, J. E. Bowers, *IEEE J. Sel. Top. Quantum Electron.* **2017**, *23*, 8200810.

[17] X. Yi, Q. F. Yang, K. Y. Yang, K. Vahala, *Opt. Lett.* **2016**, *41*, 2037.

[18] V. Brasch, M. Geiselmann, M. H. P. Pfeiffer, T. J. Kippenberg, *Opt. Express* **2016**, *24*, 29312.

[19] J. R. Stone, T. C. Briles, T. E. Drake, D. T. Spencer, D. R. Carlson, S. A. Diddams, S. B. Papp, arXiv:1708.08405 **2017**.

[20] A. Hasegawa, F. Tappert, *Appl. Phys. Lett.* **1973**, *23*, 142.

[21] L. F. Mollenauer, R. H. Stolen, J. P. Gordon, *Phys. Rev. Lett.* **1980**, *45*, 1095.

[22] S. Wabnitz, *Opt. Lett.* **1993**, *18*, 601.

[23] T. J. Kippenberg, S. M. Spillane, K. J. Vahala, *Phys. Rev. Lett.* **2004**, *93*, 083904.

[24] I. Prigogine, G. Nicolis, *J. Chem. Phys.* **1967**, *46*, 3542.

[25] L. A. Lugiato, R. Lefever, *Phys. Rev. Lett.* **1987**, *58*, 2209.

[26] W. J. Firth, in: *Soliton-driven Photonics* (Eds A. D. Boardman, A. P. Sukhorukov), Kluwer Academic, Dordrecht, **2001**, pp. 459–485.

[27] T. Ackemann, W. J. Firth, G. L. Oppo, *Adv. Atom. Mol. Opt. Phys.* **2009**, *57*, 323.

[28] J. D. Jost, T. Herr, C. Lecaplain, V. Brasch, M. H. P. Pfeiffer, T. J. Kippenberg, *Optica* **2015**, *2*, 706.

[29] P. Del'Haye, A. Coillet, T. Fortier, K. Beha, D. C. Cole, K. Y. Yang, H. Lee, K. J. Vahala, S. B. Papp, S. A. Diddams, *Nat. Photon.* **2016**, *10*, 516.

[30] M. G. Suh, Q. F. Yang, K. Y. Yang, X. Yi, K. J. Vahala, *Science* **2016**, *354*, 600.

[31] M. Yu, Y. Okawachi, A. G. Griffith, M. Lipson, A. L. Gaeta, *Opt. Lett.* **2017**, *42*, 4442.

[32] N. G. Pavlov, G. Lihachev, S. Koptyaev, E. Lucas, M. Karpov, N. M. Kondratiev, I. A. Bilenko, T. J. Kippenberg, M. L. Gorodetsky, *Opt. Lett.* **2017**, *42*, 514.

[33] D. T. Spencer, T. Drake, T. C. Briles, J. Stone, L. C. Sinclair, C. Fredrick, Q. Li, D. Westly, B. R. Ilic, A. Bluestone, N. Volet, T. Komljenovic, L. Chang, S. H. Lee, D. Y. Oh, M.-G. Suh, K. Y. Yang, M. H. P. Pfeiffer, T. J. Kippenberg, E. Norberg, L. Theogarajan, K. Vahala, N. R. Newbury, K. Srinivasan, J. E. Bowers, S. A. Diddams, and S. B. Papp, arXiv:1708.05228 **2017**.

[34] M. G. Suh, K. Vahala, arXiv:1705.06697 **2017**.

[35] P. Trocha, D. Ganin, M. Karpov, M. H. Pfeiffer, A. Kordts, J. Krockenberger, S. Wolf, P. Marin-Palomo, C. Weimann, S. Randel, W. Freude, T. J. Kippenberg, C. Koos, arXiv:1707.05969 **2017**.

[36] P. Marin-Palomo, J. N. Kemal, M. Karpov, A. Kordts, J. Pfeifle, M. H. P. Pfeiffer, P. Trocha, S. Wolf, V. Brasch, M. H. Anderson, R. Rosenberger, K. Vijayan, W. Freude, T. J. Kippenberg, C. Koos, *Nature* **2017**, *546*, 274.

[37] S. Schilt, L. Thévenaz, *Appl. Opt.* **2004**, *43*, 4446.

[38] W. Liang, D. Eliyahu, V. S. Ilchenko, A. A. Savchenkov, A. B. Matsko, D. Seidel, L. Maleki, *Nat. Commun.* **2015**, *6*, 7957.

[39] N. G. Pavlov, G. Lihachev, S. Koptyaev, A. S. Voloshin, A. D. Ostapchenko, M. L. Gorodetsky, Kerr soliton combs with regular multifrequency diode lasers, in: European Conference on Lasers and Electro-Optics (CLEO), **2017**, paper CD_11_5.

[40] K. Numata, J. Camp, M. A. Krainak, L. Stolpner, *Opt. Express* **2010**, *18*, 22781.

[41] W. Loh, F. J. O'Donnell, J. J. Plant, M. A. Brattain, L. J. Missaggia, P. W. Juodawlkis, *IEEE Photon. Technol. Lett.* **2011**, *23*, 974.

[42] T. Carmon, L. Yang, K. J. Vahala, *Opt. Express* **2004**, *12*, 4742.

[43] S. Coen, M. Erkintalo, *Opt. Lett.* **2013**, *38*, 1790.

[44] X. Yi, Q. F. Yang, K. Y. Yang, K. Vahala, *Opt. Lett.* **2016**, *41*, 3419.

[45] M. Karpov, H. Guo, A. Kordts, V. Brasch, M. H. P. Pfeiffer, M. Zervas, M. Geiselmann, T. J. Kippenberg, *Phys. Rev. Lett.* **2016**, *116*, 103902.

[46] X. Yi, Q. F. Yang, X. Zhang, K. Y. Yang, X. Li, K. Vahala, *Nat. Commun.* **2017**, *8*, 14869.

[47] D. M. Bird, J. R. Armitage, R. Kashyap, R. M. A. Fatah, K. H. Cameron, *Electron. Lett.* **1991**, *27*, 1115.

[48] G. Raybon, R. S. Tucker, G. Eisenstein, C. H. Henry, *Electron. Lett.* **1988**, *24*, 1563.

[49] P. A. Morton, V. Mizrahi, T. Tanbun-Ek, R. A. Logan, P. J. Lemaire, H. M. Presby, T. Erdogan, S. L. Woodward, J. E. Sipe, M. R. Phillips, A. M. Sergent, K. W. Wecht, *Appl. Phys. Lett.* **1994**, *64*, 2634.

[50] P. A. Morton, M. J. Morton, S. J. Morton, in: IEEE Avionics and Vehicle Fiber-Optics and Photonics Technology Conference (AVFOP), **2017**, Paper TuB.1.

[51] E. C. Cook, P. J. Martin, T. L. Brown-Heft, J. C. Garman, D. A. Steck, *Rev. Sci. Instrum.* **2012**, *83*, 043101.

[52] N. M. Kondratiev, V. E. Lobanov, A. V. Cherenkov, A. S. Voloshin, N. G. Pavlov, S. Koptyaev, M. L. Gorodetsky, *Opt. Express* **2017**, *25*, 28167.

[53] A. P. Bogatov, P. G. Eliseev, B. N. Sverdlov, *IEEE J. Quantum Electron.* **1975**, *11*, 510.

[54] H. Kalagara, P. G. Eliseev, M. Osiński, *IEEE J. Sel. Top. Quantum Electron.* **2013**, *19*, 1502508.

[55] K. Kikuchi, T. Okoshi, *IEEE J. Quantum Electron.* **1985**, *21*, 669.

[56] C. H. Henry, *IEEE J. Quantum Electron.* **1983**, *19*, 1391.

[57] R. F. Kazarinov, C. H. Henry, *IEEE J. Quantum Electron.* **1987**, *23*, 1401.

[58] K. Vahala, A. Yariv, *Appl. Phys. Lett.* **1984**, *45*, 501.

[59] S. Kobayashi, Y. Yamamoto, M. Ito, T. Kimura, *IEEE J. Quantum Electron.* **1982**, *18*, 582.

[60] J. E. Bowers, W. T. Tsang, T. L. Koch, N. A. Olsson, R. A. Logan, *Appl. Phys. Lett.* **1985**, *46*, 233.

[61] H. Lee, T. Chen, J. Li, K. Y. Yang, S. Jeon, O. Painter, K. J. Vahala, *Nat. Photon.* **2012**, *6*, 369.

[62] J. Li, H. Lee, K. Y. Yang, K. J. Vahala, *Opt. Express* **2012**, *20*, 26337.

[63] T. Herr, V. Brasch, J. D. Jost, I. Mirgorodskiy, G. Lihachev, M. L. Gorodetsky, T. J. Kippenberg, *Phys. Rev. Lett.* **2014**, *113*, 123901.

[64] T. A. Birks, Y. W. Li, *J. Lightw. Technol.* **1992**, *10*, 432.

[65] M. Cai, O. Painter, K. J. Vahala, *Phys. Rev. Lett.* **2000**, *85*, 74.

[66] S. M. Spillane, T. J. Kippenberg, O. J. Painter, K. J. Vahala, *Phys. Rev. Lett.* **2003**, *91*, 043902.

[67] P. E. Barclay, K. Srinivasan, O. Painter, *Opt. Lett.* **2005**, *13*, 801.

[68] A. B. Matsko, W. Liang, A. A. Savchenkov, D. Eliyahu, L. Maleki, *Opt. Lett.* **2016**, *41*, 2907.

[69] K. E. Webb, M. Erkintalo, S. Coen, S. G. Murdoch, *Opt. Lett.* **2016**, *41*, 4613.

[70] V. E. Lobanov, G. V. Lihachev, N. G. Pavlov, A. V. Cherenkov, T. J. Kippenberg, M. L. Gorodetsky, *Opt. Express* **2016**, *24*, 27382.

[71] H. Guo, M. Karpov, E. Lucas, A. Kordts, M. H. P. Pfeiffer, V. Brasch, G. Lihachev, V. E. Lobanov, M. L. Gorodetsky, T. J. Kippenberg, *Nature Phys.* **2017**, *13*, 94.

[72] M. Erkintalo, S. Coen, *Opt. Lett.* **2014**, *39*, 283.

[73] H. Lee, M. G. Suh, T. Chen, J. Li, S. A. Diddams, K. J. Vahala, *Nat. Commun.* **2013**, *4*, 1.